MINERALOGICAL MAGAZINE, DECEMBER 1983, VOL. 47, PP. 453-63

Pyrrhotine–pentlandite ore textures: a mechanistic approach

D. P. KELLY AND D. J. VAUGHAN

Department of Geological Sciences, University of Aston in Birmingham, Birmingham B4 7ET

ABSTRACT. The kinetics and mechanisms of pentlandite [$(Fe,Ni)_9S_8$] exsolution from the monosulphide solid solution [or *MSS* $(Fe,Ni)_{1-x}S$] have been studied by synthesis and annealing experiments in part of the Fe–Ni–S system particularly relevant to sulphide nickel orebodies. This experimental work has been combined with the examination of the compositions and textures of pyrrhotine–pentlandite intergrowths from a variety of ore deposits. Isothermal annealing of *MSS* compositions with varying *M*:S and Fe:Ni ratios at 400 °C shows the formation of a sequence of textures which depend for their full development chiefly on initial *M*:S ratio and annealing time. The full sequence of textures starts with heterogeneous nucleation of pentlandite at *MSS* grain boundaries, the growth of these blebs to form 'rims', nucleation of finer bladed particles arranged 'en échelon' along fractures, and, finally, homogeneous nucleation of fine orientated pentlandite lamellae. Using the information from the annealing experiments, the intergrowths produced by cooling in the natural ores are interpreted using a simplified Time-Temperature-Transformation Model.

THE importance of an understanding of ore textures has been recognized in numerous studies of the textures observed in individual ore deposits at the macroscopic and microscopic levels as summarized in various texts and reference works (e.g. Edwards, 1947; Ramdohr 1969, 1981). The more recent texts have emphasized the importance of studies of the phase equilibria in relevant systems to textural interpretation (e.g. Craig and Vaughan, 1981). However, although phase equilibria have been studied in a wide variety of ore mineral systems and these studies have helped in the overall problem of textural interpretation, their application to the understanding of textures does have severe limitations. This is largely because phase equilibrium studies provide a very incomplete and idealized picture of mineral behaviour, characterizing only the final equilibrium state. In natural ore mineral systems, the *mechanisms* and *rates* of reactions will have a very important influence on the textures which result in any particular case. New approaches are therefore needed in the experimental and theoretical study of ore textures, especially those which involve exsolution processes. Potentially, such new approaches may lead not only to a better understanding of the origins of the textures observed in many ores, but also to further applications of textural studies in estimating rates of cooling and of diffusion within and throughout orebodies. The aim of this paper is to outline the methods and the concepts we have used in experimental studies of the Fe–Ni–S system, a system relevant to the formation of the pentlandite–pyrrhotine ore textures which are characteristic of the so-called 'sulphide nickel' deposits. After describing some initial results on the kinetics and mechanisms of pentlandite exsolution in the Fe–Ni–S system, these results will be used to provide a model for the interpretation of textures observed in the natural ores.

Examples of sulphide nickel ore bodies occur in a variety of geological environments and include: the Sudbury Basin, Ontario, Canada (Hawley and Haw, 1957, Hawley, 1962); the Noril'sk–Talnakh deposits of Northern Siberia, USSR (Smirnov, 1977); the Kotalahti–Hitura deposits, Finland (Papunen, 1970); the Insizwa deposit, Southern Africa (Tischler *et al.*, 1981); the Pikwe–Selebi deposits, Botswana (Lear, 1979); and the Kambalda deposits of Western Australia (Gresham and Loftus-Hills, 1981). Suggested classification schemes for these deposits are given by Naldrett and Cabri (1976), Naldrett (1979), and Ross and Travis (1981). Most workers consider these ores to have formed by the separation of an immiscible sulphide liquid from a parent mafic or ultramafic silicate magma with subsequent crystallization of sulphides from the melt. Mechanisms of sulphide separation and partitioning of elements between sulphide and silicate liquid are discussed in Duke and Naldrett (1978), Rajamani and Naldrett (1978), and Boctor (1981). In deposits such as those of the Sudbury Basin, the textures resulting from the crystallization of the immiscible sulphide liquid and the subsolidus transformations which occurred on further cooling

appear to have been preserved. In contrast, deposits such as those at Kambalda have been subjected to dynamothermal metamorphism up to amphibolite facies and this has led to extensive recrystallization of the ore minerals and to textural changes (Barrett *et al.*, 1977; Ostwald and Lusk, 1978; Marston and Kay, 1980).

The theoretical concepts used in describing and interpreting the synthetic and natural textures will not be discussed here in any detail. They can be found in reviews such as Chadwick (1972), Martin and Doherty (1976), Nicholson (1970), Greenwood (1969), Manning (1973), and Gjostein (1973). Texts and articles with a greater mineralogical emphasis include Yund and McCallister (1970), Yund and Hall (1970), McConnell (1975), Champness and Lorimer (1976), and, in particular, Putnis and McConnell (1980).

Experimental studies of the Fe-Ni-S system

Previous work. The phase relations in the Fe-Ni-S system have been studied by a number of authors, more recently including Kullerud (1963), Naldrett *et al.* (1967), Shewman and Clark (1970), Misra and Fleet (1973*a*), Craig (1973), and through compilations of Barker (pers. comm. 1981).

From 900 °C down to 270 °C the system is dominated by a complete solid solution from $Fe_{1-x}S$ to $Ni_{1-x}S$ termed the *monosulphide solid solution* or *MSS* (see fig. 1). Pentlandite $(Fe,Ni)_9S_8$ becomes stable at 610 °C in a compositional range where no liquid is present. Below ~ 270 °C the *MSS* breaks down and eventually disappears completely; reports of the temperature at which this occurs vary, illustrating the difficulty of obtaining equilibrium below ~ 300 °C.

The bulk compositions of the sulphide fraction of many sulphide nickel orebodies plot within the *MSS*, generally towards more Fe-rich compositions ($\lesssim$ 20 at %), when plotted in terms of the Fe-Ni-S system (Naldrett *et al.*, 1967). This indicates that the bulk of the sulphides in these ores initially crystallized as *MSS*, which remained homogeneous on cooling to temperatures in the region of 500–600 °C. The subsolidus process which thereafter produces pentlandite can be illustrated by considering fig. 2. Here the iron-rich and sulphur-poor portion of the *MSS* is shown in terms of atomic percent S plotted against atomic percent Ni (the compositional field in which pentlandite occurs is shifted by 10 atomic percent to the left—a necessary convenience for drafting). In addition to the sulphur-poor limits of the *MSS* (data from Naldrett *et al.*, 1967) for 600, 400, and 300 °C, the plot shows a series of *MSS* compositions which were synthesized in this work (as discussed below). From this it can be seen that, as the temperature

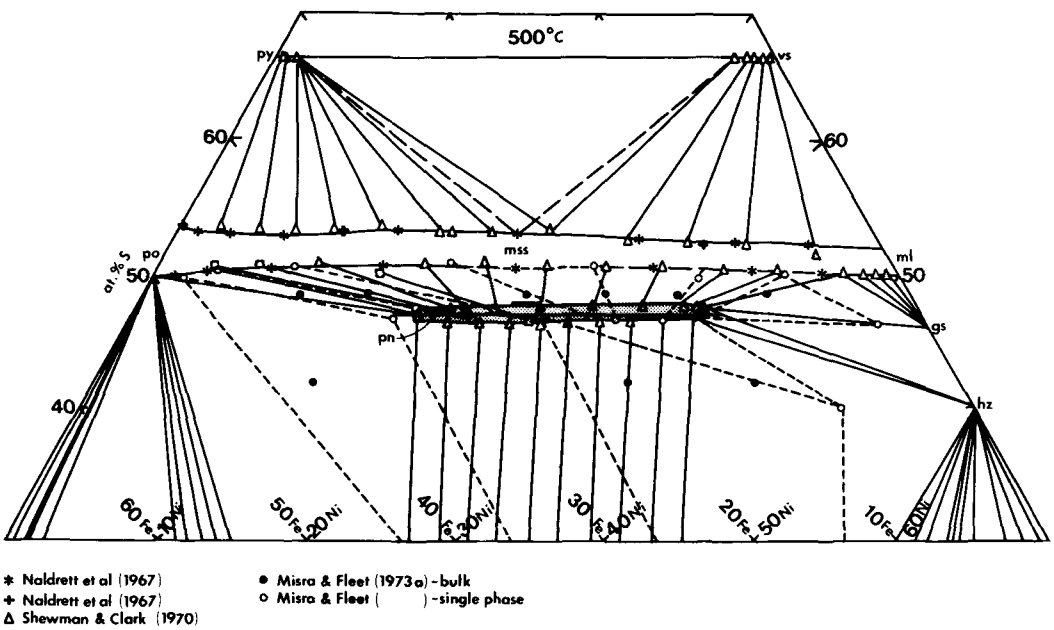

FIG. 1. Phase relations in the central portion of the Fe-Ni-S system at 500 °C (compiled by Barker (pers. comm. 1980) from published data).

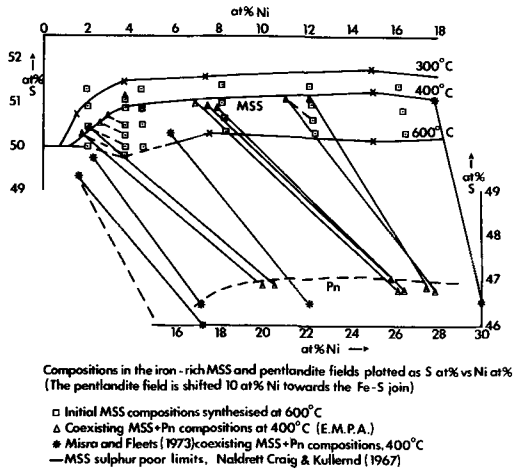

FIG. 2. Compositions in the Fe-rich *MSS* and pentlandite (pn) fields plotted as S at % *vs.* Ni at %.

decreases below 600 °C, the *MSS* field retreats to more sulphur-rich compositions. Hence, when samples synthesized in this work were annealed at 400 °C, the originally homogenous *MSS* compositions exsolved a more Ni-rich pentlandite and moved towards more Ni-poor and Fe- and S-rich compositions. Phase equilibria studies indicate, therefore, that on cooling of sulphide nickel ores below 600 °C, the originally homogenous *MSS* will exsolve a more Ni-rich pentlandite. As cooling and exsolution proceeds this will leave the residual *MSS* matrix progressively more Fe- and S-rich until eventually it stabilizes as pyrrhotine. A more complete understanding of the ore textures produced by this exsolution requires a consideration of kinetic and mechanistic factors. Progress in this area has recently been made by Durazzo and Taylor (1982) who undertook experimental studies of textures developed in the Fe–Ni–S system; we have examined a wider range of *MSS* compositions and used longer maximum annealing times in the present work.

This study. In order to study the kinetics and mechanisms of pentlandite exsolution, a series of *MSS* compositions of varying Fe:Ni and *M*:S ratios were synthesized as illustrated in fig. 2. These compositions were prepared using high purity iron, nickel, and sulphur powders in sealed evacuated silica glass tubes using techniques described by Kullerud (1971) and Scott (1974). Homogeneity and composition of the products were checked by reflected light microscopy, X-ray diffraction and electron probe microanalysis. Microscopy revealed that the individual *MSS* grains ranged in size from 50–500 μm. Aggregates of grains made up polygonal mosaics showing 120° triple junctions (fig. 5*a*). Each synthesized *MSS* composition was subdivided into batches which were annealed in isothermal runs at 400 °C varying in duration from 1 h to 3 months. This enabled both the rate of reaction and the evolution of the textures produced to be monitored. Although only data obtained from the 400 °C runs will be reported here, further work is being undertaken at lower temperatures.

Pentlandite–MSS exsolution textures in the Fe–Ni–S system

The compositions of the *MSS* phases are very different from that of pentlandite and so are the respective crystal structures, the former having the NiAs-type structure (Francis, 1974; Misra and Fleet 1973*b*) and the latter an unusual cubic structure with most of the metals in tetrahedral coordination (Rajamani and Prewitt, 1973; Vaughan and Craig, 1978). Because of this, exsolution involves a nucleation event with the agglomeration and stabilization of small clusters of atoms with the pentlandite structure occurring within the *MSS* matrix. Clearly, this also involves the diffusion of Fe and Ni and, to a lesser extent, S atoms through the *MSS* lattice. In order for the formation of pentlandite within the *MSS* to occur, there must be a driving force for the nucleation event.

Fig. 3 shows a *T*–*X* section along a tie-line linking two of the coexisting *MSS* compositions in fig. 2. This shows the sulphur-poor boundary of the *MSS* or *MSS*-pentlandite solvus shifting to lower *M*:S ratios as the temperature decreases. Consider a composition of *M*:S = 0.974:1 (50.65 at %S). It can be seen that this lies on the equilibrium *MSS*-pentlandite solvus at $\simeq$ 500 °C and here the

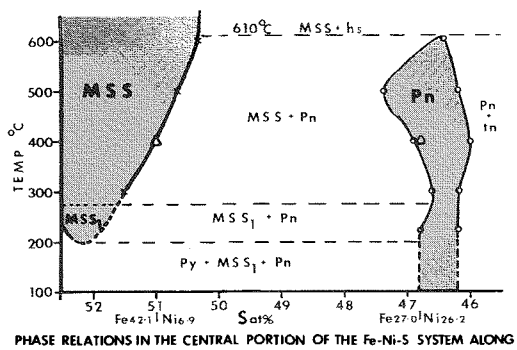

FIG. 3. Temperature (*T*)-composition (*X*) section across the *MSS* and pentlandite fields, along a tie-line linking (*MSS*)$Fe_{42.1}Ni_{6.9}S_{52.0}$ and (pn) $Fe_{27.0}Ni_{26.2}S_{46.8}$ (at %).

free energy of the system is at a minimum so that there is no driving force for exsolution. At 400 °C, the M : S ratio for an equilibrium *MSS* composition is 0.960 : 1 (51.0 at %S). The composition with M : S of 0.974 : 1 now lies below the equilibrium *MSS*–pentlandite solvus and there is now a net driving force ($-\Delta G_{vol}$) for the *MSS* to shift composition from 0.974 to 0.960. Thus, by exsolving pentlandite the *MSS* moves towards the equilibrium composition, thereby lowering the free energy of the system. So for exsolution to proceed, there must be a degree of undercooling below the equilibrium *MSS*–pentlandite solvus and, as undercooling increases, so does the driving force for exsolution ($-\Delta G_{vol}$). It can be appreciated that in a series of isothermal experiments, by increasing the M : S ratio of the *MSS* composition, the driving force for nucleation is being increased and this is equivalent to increasing the degree of undercooling. This is clearly illustrated by fig. 4, in which the volume fraction of pentlandite exsolved is shown as a function of time for a series of *MSS* compositions with the same Fe : Ni ratio but different M : S ratios. The data show that the exsolution rate (and hence the driving force for nucleation) increases as the initial M : S ratio increases. Thus, for the composition with a metal to sulphur ratio of 0.955 : 1, the equilibrium *MSS*–pentlandite solvus has not been crossed at 400 °C so that no pentlandite has been exsolved. As the ratio increases to 1 : 1, the rate of exsolution progressively increases.

The products of the isothermal runs at 400 °C can also be used to examine the types of textures produced. These are also found to depend on the initial M : S ratio of the *MSS* since this dictates the degree of undercooling and value of $-\Delta G_{vol}$. These phenomena arise because of two positive free energy terms ($+\Delta G_{strain}$ and $+\Delta G_{surface}$) which oppose $-\Delta G_{vol}$ and which result from the creation within the *MSS* matrix of small areas of different structure—the nuclei of pentlandite grains. The

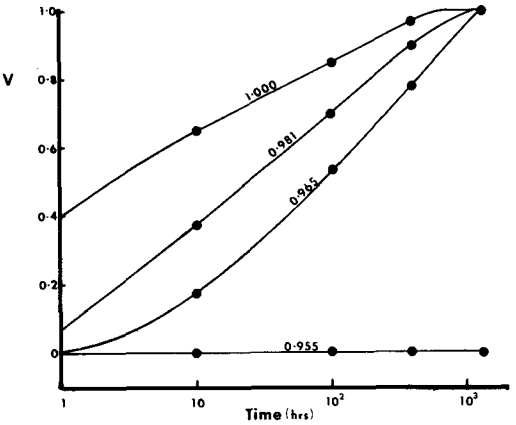

DIAGRAM ILLUSTRATING THE DEPENDANCE OF THE PENTLANDITE EXSOLN. RATE ON THE INITIAL M:S RATIO, FOR MSS COMPOSITIONS OF THE SAME Fe:Ni RATIO.(12·3±3·7at% Ni). Temperature 400°c. Volume fraction of Pn exsolved (V) vs Time(log scale).

FIG. 4. Volume fraction of pentlandite exsolved (V) with time (log scale), at 400 °C, for four *MSS* compositions synthesized with the same Fe : Ni ratio ($\approx$ 12.3) but differing M : S ratios.

magnitudes of these terms will depend on the degree of matching or mismatching (coherency) of crystal lattices across the interface between the pentlandite nuclei and the matrix. Preferential nucleation of pentlandite at defects (grain boundaries, fractures, etc.) within the *MSS* matrix will offset these terms by partially removing the positive free energy term associated with the defect. The greatest saving in free energy will be achieved by such heterogeneous nucleation at grain boundaries. The overall evolution of the textures produced in the experiments at 400 °C are illustrated in figs. 5 and 6 and the development of these textures as functions of both time and initial M : S ratio for a series of compositions of the same Fe : Ni ratio is shown in fig. 7.

Heterogeneous nucleation of pentlandite at *MSS*

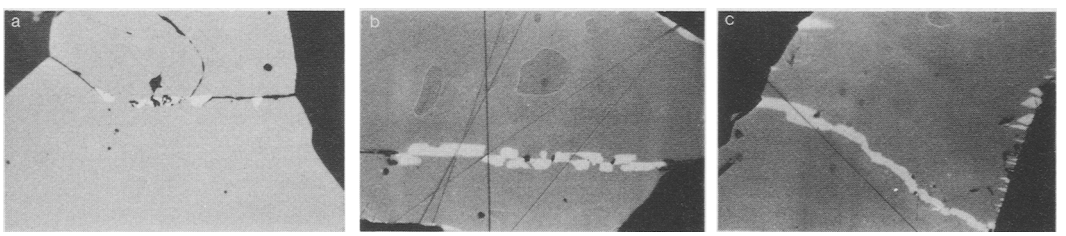

FIG. 5. Photomicrographs illustrating the development of pentlandite textures in isothermal runs at 400 °C. (Each photograph was taken in PPL using an oil immersion objective; the field of view is 130 μm.) (*a*) Discrete hemispherical pentlandite blebs at *MSS* grain boundary (Fe : Ni = 5 : 1; M : S = 0.973 : 1; 10 h). (*b*) Lozenge-shaped pentlandite blebs either side of *MSS* grain boundary (Fe : Ni = 5 : 1; M : S = 0.981 : 1; 10 h). (*c*) Growth and impingement of pentlandite lozenges developing rim pentlandite along *MSS* grain boundary. Orientated pentlandite blades at grain margin. (Fe : Ni = 5 : 1; M : S = 0.981 : 1; 100 h).

grain boundaries results initially in the formation of discrete hemispherical blebs (fig. 5*a*); the morphology suggests an incoherent interface between pentlandite particles and *MSS* matrix. The precise natures of the interfaces are presently being studied using Transmission Electron Microscopy. In the case of compositions of higher M : S ratio, the blebs are lozenge shaped (fig. 5*b*), perhaps indicating a more coherent interface. The strain energy associated with this interface would be overcome by the higher driving force for nucleation. Further nucleation and growth results in the impingement of these particles and the formation of continuous rims of pentlandite along *MSS* grain boundaries. Fig. 5*c* shows overgrowth and impingement of discrete blebs either side of a grain boundary. At this stage orientated blades or lobate blebs also form at grain margins; the proportion of blades being higher with the highest initial M : S ratios, where blades at grain boundaries not already occupied by rim pentlandite are also found. Growth of these textures continues and produces, in the case of rim pentlandite, more continuous and wider rims (figs. 6*a*, *b*). Compositions with a Fe : Ni ratio of 5 : 1 and the lowest M : S ratio (0.961 : 1) show observable pentlandite particles after $\sim$ 500 h and only rim pentlandite is ever produced. For an intermediate M : S ratio (0.973 : 1), pentlandite rims are observed after 100 h and pentlandite blades or blebs after 500 h. At the highest M : S ratio (0.981 : 1) this stage is reached after only $\sim$ 10 h. Further nucleation and growth occurs in the compositions of highest initial M : S ratio with the formation of finer blades orientated 'en échelon' along fractures, and in some cases, to the formation of bladed extensions from pentlandite rims (fig. 6*a*). Finally, homogeneous

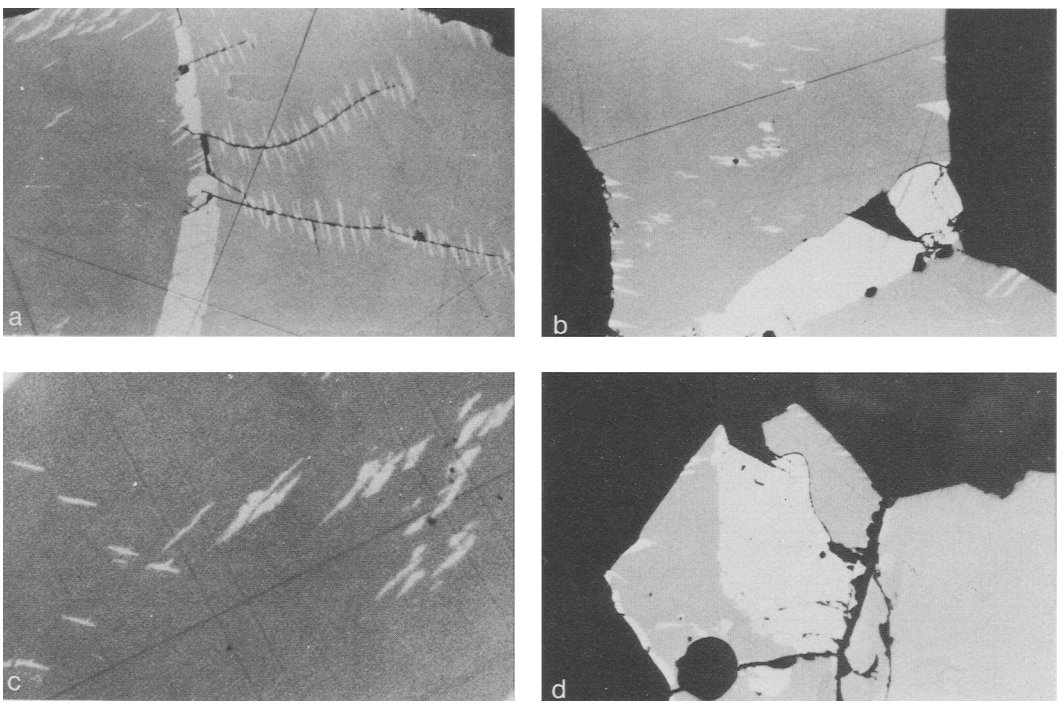

FIG. 6. Photomicrographs illustrating the development of pentlandite textures in isothermal runs at 400 °C (conditions and magnifications as in fig. 5): (*a*) Pentlandite rim with fine bladed extensions at *MSS* grain boundary. Pentlandite blades orientated 'en échelon' along fractures within *MSS* grain. Pentlandite blades (note difference in orientation between adjacent grains) at grain margins (Fe : Ni = 5 : 1; M : S = 0.981 : 1; 500 h); (*b*) Relatively coarse continuous pentlandite rim at *MSS* grain boundary. Coarsened lamellae orientated in one direction within *MSS* grain. Pentlandite blades at grain margins. (Fe : Ni = 5 : 1; M : S = 0.981 : 1; 1780 h); (*c*) Coarsening of one set of parallel pentlandite lamellae in direction perpendicular to their elongation results in impingement of adjacent lamellae and formation of pentlandite 'flames'. Second set of finer lamellae orientated at 60° to first show no evidence of coarsening (Fe : Ni = 5 : 1; M : S 0.981 : 1; 1780 h).; (*d*) Coarse granular pentlandite approximately the same grain-size as two adjacent relatively small *MSS* grains. Part of larger *MSS* grain is visible on the right. (Fe : Ni = 3 : 1; M : S 0.973 : 1; 1780 h).

nucleation of pentlandite occurs in areas of host *MSS* which are free from any visible defects and this produces pentlandite lamellae within *MSS* grains which are usually orientated in one direction in the *MSS* host (figs. 6*b*, *c*) but occasionally in three directions at 60° to each other.

X-ray studies on a limited number of natural and synthetic samples by Francis *et al.* (1976) indicate that these orientations represent matching along crystallographic planes as follows: (111) pentlandite // (00.1) *MSS*, ($0\bar{1}1$) pentlandite // (11.0) *MSS*, ($\bar{1}\bar{1}2$) pentlandite // (10.0) *MSS*. The greatest degree of lattice match (coherency) occurs for the orientation (111) pentlandite // (00.1) *MSS*. This orientation will therefore be energetically more favourable. With further annealing and growth a decrease in free energy will be attained if these lamellae lose coherency. Coarsening occurs in a direction perpendicular to their direction of elongation and this leads to impingement of adjacent lamellae and the formation of 'flame-like' intergrowths similar to those observed in natural samples (fig. 6*c*, cf. fig. 9*c*).

Other growth and coarsening features observed include the impingement of adjacent lobate blebs and blades to form larger blocky pentlandite areas at grain margins and the formation of very coarse granular areas of pentlandite (fig. 6*d*) in compositions of Fe : Ni $\leqslant$ 3 : 1 with intermediate to high *M* : S ratios.

Textures and compositions of some natural pyrrhotine–pentlandite intergrowths

In parallel with the experimental studies of the Fe–Ni–S system outlined above, examples of pyrrhotine–pentlandite intergrowths from sulphide nickel deposits have been studied in polished section and using electron probe microanalysis.

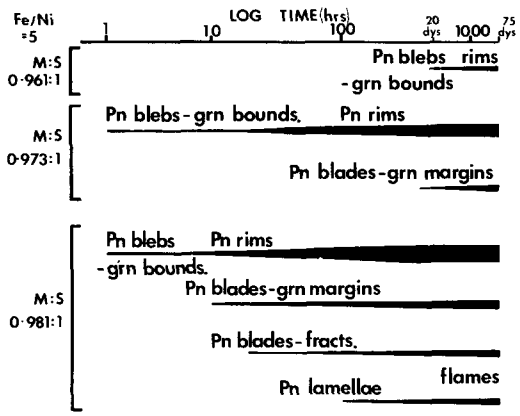

FIG. 7. Development of pentlandite textural types with time at 400 °C for three *MSS* compositions of the same Fe : Ni ratio (5 : 1) but differing *M* : S ratios.

The full range of textures observed within and between different orebodies will be discussed in detail elsewhere. However, in those ores which have not been subjected to any significant metamorphism or recrystallization, the textures observed are remarkably similar to many of those produced in the experimental work and described above. Textures observed in some of the Sudbury ores are illustrated in figs. 8 and 9. These include the characteristic rim pentlandite along pyrrhotine grain boundaries (figs. 8*a*, *b*). Notable in these textures is a decrease in width of the rims with decrease in grain-size of the pyrrhotine mosaic and also the occurrence of more granular pentlandite at pyrrhotine triple junctions (fig. 8*b*). In the very fine-grained pyrrhotine mosaics which occur in disseminated ores, complete segregation of pentlandite may occur to form discrete interstitial grains (fig. 8*c*). Other textural types include the flame pentlandites which are, in fact, aggregates of finer pentlandite particles, the overall morphology of which varies depending upon the site at which they are developed. For instance, flames developed at grain boundaries commonly consist of series of sub-parallel, partially agglomerated, elongate blades or plates (fig. 9*a*) and when developed either side of a grain boundary give rise to a herringbone or dendritic intergrowth (fig. 9*b*). On the other hand, flames developed within pyrrhotine grains at areas free from any visible defect consist of a series of elongate blebs, lozenges, and lamellae orientated at low angles to the direction of elongation of the rod-like flame (fig. 9*c*). Other flame-types include extensions to pentlandite rims and more bladed aggregates arranged 'en échelon' along fractures within the pyrrhotine grains (fig. 9*d*). The proportion of the flame pentlandites found within pyrrhotine grains markedly increases in grains $\geqslant$ 2000 μm in diameter. Within any one pyrrhotine grain, the flames are all orientated sub-parallel to one another, and sub-parallel to the pyrrhotine basal parting where this is developed. Determinations of this orientation relationship using the optical scheme of Kanehira (1969) suggest that the flames are elongate perpendicular to the trace of the *c* axis within any one pyrrhotine section.

Studies of the pyrrhotines in the Sudbury ores have confirmed that they are commonly made up of what appears to be a two-phase intergrowth when observed under the reflected light microscope. Fig. 8*d* was taken on an unetched specimen using a Zeiss photomicroscope II under completely crossed polars with a high level of incident illumination. Careful electron microprobe analysis of selected and photographed areas within individual polished

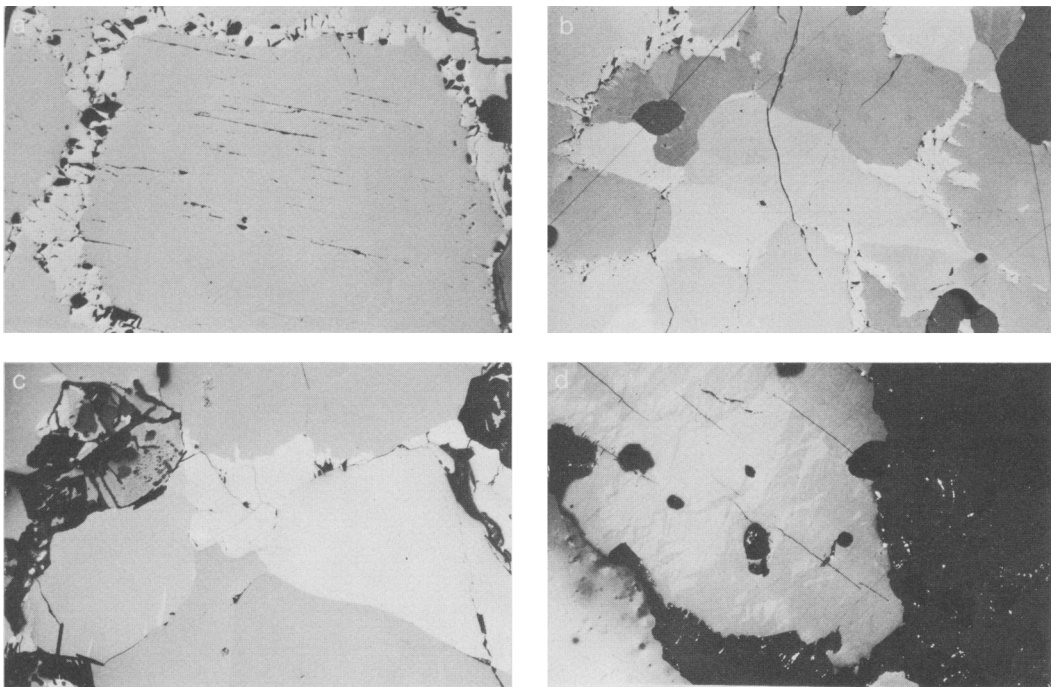

FIG. 8. Pentlandite/pyrrhotine ore textures from Strathcona and Copper Cliff mines, Sudbury, Ontario: (*a*) Coarse rim pentlandite around margin of large pyrrhotine grain. (Field of view 3.4 mm, PPL); (*b*) Finer-grained pyrrhotine mosaic with thinner discontinuous pentlandite rims. More granular pentlandite is developed at triple junctions. (Field of view 3.4 mm, PPL); (*c*) Discrete interstitial pentlandite grain within mosaic of fine ~ 200 μm pyrrhotine grains. Note also fine acicular pentlandite flames at grain boundary (lower left). (Field of view 500 μm; partially crossed polars; oil immersion); (*d*) Concentration of monoclinic pyrrhotine (darker grey) adjacent to pentlandite at pyrrhotine grain margin while the core of the grain is dominantly 'hexagonal' pyrrhotine (lighter grey). (Field of view 2 mm; crossed polars.)

sections show that the darker phase has a composition ~ $(Fe,Ni)_7S_8$ consistent with monoclinic pyrrhotine, whereas the lighter phase of composition ~ $(Fe,Ni)_{10}S_{11}$ is presumably 'hexagonal' pyrrhotine (see Table I). Subsequent etching of these areas with magnetic colloid confirmed that the darker phase is ferrimagnetic and therefore monoclinic pyrrhotine. In fact, X-ray and electron diffraction studies of pyrrhotines indicate that although they tend to fall into narrow compositional ranges around Fe_7S_8 and between Fe_9S_{10}–$Fe_{10}S_{11}$ (Carpenter and Desborough, 1964; Arnold, 1967; Morimoto *et al.*, 1975), within each compositional range, fine scale intergrowths of various pyrrhotine superstructure types occur. At Fe_7S_8, $4C+nC$ (monoclinic pyrrhotine + intermediate hexagonal pyrrhotines), and from Fe_9S_{10} to $Fe_{10}S_{11}$, various nC types occur. The notation (after Wuensch, 1963) refers to the repeat of the basic NiAs-type unit cell along the c axis which characterizes the superstructure, n being a non-integral repeat.

The monoclinic phase, as noted by Vaughan *et al.* (1971), is concentrated at grain margins, particularly those adjacent to areas of rim pentlandite (fig. 8*d*). The centres of the grains are dominantly made up of 'hexagonal' pyrrhotine, with a lamellar to patchy intergrowth of the monoclinic phase. Flame pentlandite developed within the pyrrhotine grains, whether at fractures or defect-free areas, is invariably enveloped in a thin sheath of monoclinic pyrrhotine which is elongated parallel to the flame. This was first commented on by Naldrett *et al.* (1967). This distribution pattern is best developed in larger ($\geqslant$ 800 μm) grains within massive ores. In some disseminated ores, the proportion of the monoclinic phase is higher and results in a barely discernible fine lamellar intergrowth throughout the grains. Similar 'hexagonal' and monoclinic pyrrhotine intergrowths have been observed in other sulphide nickel orebodies, e.g. Kotalahti, Finland (Papunen, 1970); Selebi-Pikwe, Botswana (Lear, 1979).

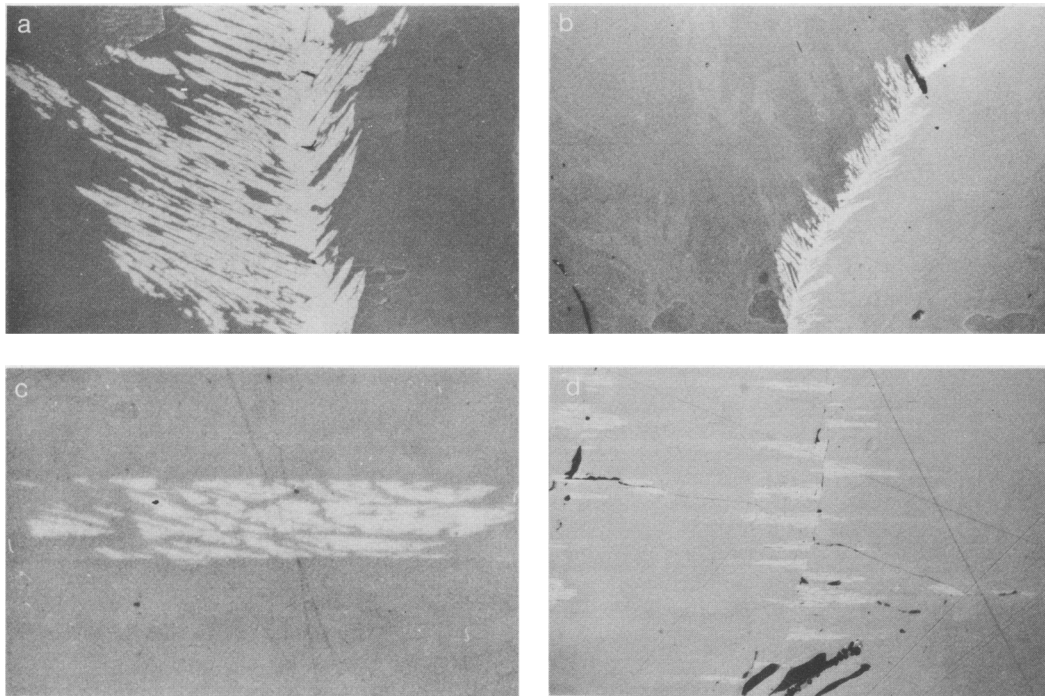

FIG. 9. Flame-type pentlandites from the Strathcona and Copper Cliff mines, Sudbury, Ontario; (*a*) Series of sub-parallel partially agglomerated blades of plates of pentlandite at pyrrhotine grain boundary. (Field of view 160 μm; PPL; oil immersion); (*b*) Dendritic or herring-bone pentlandite at pyrrhotine grain boundary. Note difference in orientation of blades in the adjacent pyrrhotine grains. (Field of view 500 μm; nearly cross polars; oil immersion); (*c*) Flame pentlandite within defect-free area of pyrrhotine grain. The flame consists of a series of finer pentlandite particles such as elongate lozenges, blebs and lamellae orientated at low angles to the direction of elongation of the flame. (Field of view 130 μm; PPL; oil immersion); (*d*) Flame pentlandites orientated 'en échelon' along a fracture within a pyrrhotine grain. (Field of view 500 μm; PPL; oil immersion.)

Electron probe microanalyses of the pyrrhotines in the Sudbury ores (see Table I and Vaughan *et al.*, 1971; Batt, 1972) show that the hexagonal phase consistently has approximately double the amount of 'residual' nickel compared to the monoclinic phase. This, together with the association of monoclinic pyrrhotine adjacent to pentlandite, suggests that ordering and exsolution within the pyrrhotines is intimately related to the final stages of pentlandite exsolution and growth. Studies of self-diffusion in pyrrhotine (Condit *et al.*, 1974) and $Ni_{1-x}S$ (Klotsman *et al.*, 1963) at temperatures down to 277 °C indicate that the sulphur diffusion rate is several orders of magnitude lower than that of Fe or Ni. Therefore below ~ 240 °C during final stages of pentlandite exsolution, growth and compositional change, diffusion of sulphur out from the grain margins would take place over relatively short distances leaving the pyrrhotine grain margins sulphur-enriched. Restricted exchange of Ni into, and Fe away from, the adjacent pentlandite results in Ni depletion within this area. Similar, smaller scale, S-enriched and Ni-depleted areas would also occur around pentlandite flames. At the same time, transformation of these S-enriched areas to a dominantly 4*C*-type pyrrhotine of composition $(Fe,Ni)_7S_8$ would occur while the more metal-rich core of the grains would transform to a mixture of intermediate *nC* pyrrhotines (of Fe_9S_{10}–$Fe_{10}S_{11}$ composition) with lamellar intergrowths of 4*C*-type by vacancy ordering and exsolution as suggested by Putnis and McConnell (1980).

Pentlandite compositions in the samples analysed are remarkably homogeneous. There is no evidence for zoning within even the larger pentlandite rims, or between pentlandites in different areas of the same sample, or between different pentlandite textural types (although it is obviously difficult to get accurate analysis of flame pentlandites). This is consistent with previously published pentlandite

Table I. Electron probe Analyses of Sulphides from copper Cliff, Sudbury, Ontario (all values in wt.%)*

Sample Number and Species	S	Fe	Ni	Co	Cu	Total	Structural Formula
CC8 Mono.pyrrhotine	39.51	60.45	0.31	0.11	0.06	100.44	$(Fe_{7.03}Ni_{0.03}Co_{0.01})_{7.06}S_8$
" Hex. pyrrhotine	38.82	60.80	0.73	0.13	0.07	100.55	$(Fe_{9.89}Ni_{0.11}Co_{0.02})_{10.02}S_{11}$
" Pentlandite	33.30	30.88	35.15	1.26	0.12	100.70	$(Fe_{4.26}Ni_{4.61}Co_{0.16}Cu_{0.01})_{9.04}S_8$
CC13 Mono.pyrrhotine	40.04	60.93	0.36	0.09	-	101.42	$(Fe_{6.99}Ni_{0.04}Co_{0.01})_{7.04}S_8$
" Hex pyrrhotine	39.33	61.26	0.74	0.09	-	101.42	$(Fe_{8.94}Ni_{0.10}Co_{0.01})_{9.05}S_{10}$
" Pentlandite	33.44	31.08	35.80	0.94	-	101.26	$(Fe_{4.27}Ni_{4.68}Co_{0.12})_{9.07}S_8$
CC20 Mono. pyrrhotine	39.65	60.57	0.40	0.13	0.08	100.83	$(Fe_{7.02}Ni_{0.04}Co_{0.01})_{7.07}S_8$
" Hex. pyrrhotine	38.99	61.04	0.78	0.13	0.07	101.01	$(Fe_{9.87}Ni_{0.12}Co_{0.02})_{10.01}S_{11}$
" Pentlandite	33.27	30.90	35.39	1.16	0.11	100.83	$(Fe_{4.29}Ni_{4.65}Co_{0.15}Cu_{0.01})_{9.08}S_8$
CC28 Mono.pyrrhotine	39.59	60.49	0.35	0.13	0.06	100.62	$(Fe_{7.01}Ni_{0.03}Co_{0.01})_{7.05}S_8$
" Hex. pyrrhotine	38.93	60.86	0.80	0.11	0.07	100.70	$(Fe_{9.87}Ni_{10.12}Co_{0.01})_{10.00}S_{11}$
" Pentlandite	33.03	30.89	35.86	1.12	0.15	100.44	$(Fe_{4.29}Ni_{4.66}Co_{0.15}Cu_{0.02})_{9.12}S_8$

* Cambridge Instruments Microscan V, accelerating voltage 15 kV, specimen/probe current 0.05 . Standards: synthetic FeS, synthetic NiS, synthetic $Cu_{0.5}Co_{2.5}S_4$ (carrollite), synthetic CuS. Ten separate ten second counts were made to determine the average count rate for each element in the individual spot analyses. ZAF corrections applied using the methods of Sweatmen and Long (J. Petrol. 10, 332, 1969). The mineral analyses quoted are the average of at least ten individual spot analyses.

analyses (e.g. Misra and Fleet, 1973*a*; Harris and Nickel, 1972).

Discussion

The experimental results can be used to interpret qualitatively the progressive development of natural textures by means of a schematic Time-Temperature-Transformation (*T-T-T*) diagram (fig. 10). This represents the processes occurring along a cooling path *A-B*, in material of a particular bulk composition which intersects the equilibrium *MSS*-pentlandite solvus at temperature *Tc*. To a first approximation the experimental results for a given bulk composition, such as presented in fig. 7, represent an isothermal section through such a diagram. Further isothermal runs, which are under way, will enable us to quantify this isothermal *T-T-T-X* model. However, it should be noted that a continuous cooling *T-T-T* diagram differs slightly from an isothermal *T-T-T* diagram by having the curves shifted to lower temperatures and longer times (Putnis and McConnell, 1980; Uhlmann *et al.*, 1975). Additional factors affecting the kinetics will be the grain size of the *MSS*, and the presence in natural materials of impurities such as As, Sb, and Bi, which inhibit diffusion or exert a drag effect on grain growth (Polmear, 1966; Yund and Hall, 1970) by segregating into the pentlandite/*MSS* interface. Despite these complexities, the sequence of heterogeneous nucleation followed by homogeneous nucleation (fig. 10*a*) qualitatively succeeds in explaining the textures already described from the Sudbury ores.

Heterogeneous nucleation initially occurs at grain boundaries leading to the development of rim pentlandite (fig. 8*a*). With slow cooling these may develop into more granular pentlandite at triple junctions (fig. 8*b*). In finer grained mosaics of *MSS*, smaller diffusion distances are involved so

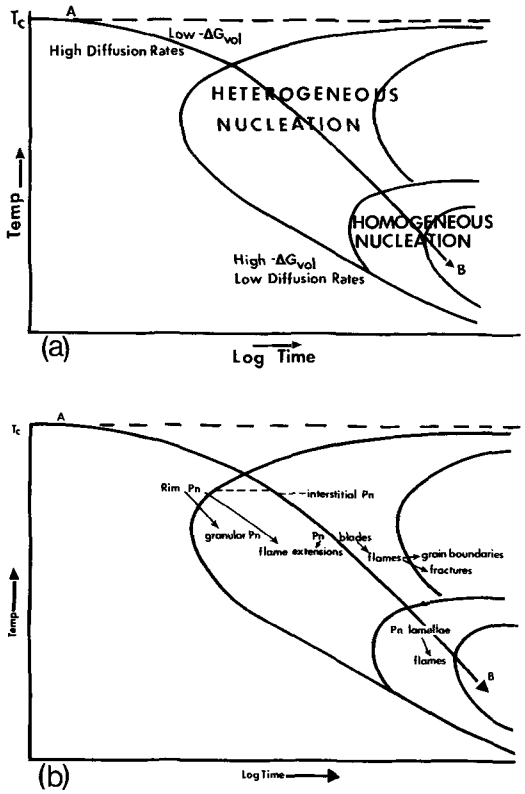

FIG. 10(*a*). Schematic Time-Temperature-Transformation (*T-T-T*) diagram illustrating the relative positions of the curves for initiation and completion of heterogeneous and homogeneous nucleation. (*b*) Schematic *T-T-T* diagram summarizing the development of the natural pentlandite/pyrrhotine intergrowths described in the text.

that complete segregation of interstitial pentlandite grains may occur. Compositional homogeneity will be maintained to low temperatures through inter-diffusion of nickel and iron along 'short circuit' diffusion paths such as grain boundaries.

As cooling continues, volume diffusion of Fe, Ni, and S withing *MSS* grains decreases exponentially (Condit *et al.*, 1974; Klotsman *et al.*, 1963). Therefore compositional changes required within the *MSS* matrix will become increasingly difficult, leading to further undercooling and departure from 'equilibrium'. Heterogeneous nucleation of orientated pentlandite particles becomes possible giving flame-like bladed particles at grain boundaries (fig. 9*a*, *b*) or as extensions to previously formed pentlandite rims. These will be orientated along planes of least mismatch, thereby reducing the strain energy involved in growth. The increased driving force for nucleation allows flames to form at less potent defects such as fractures (fig. 9*d*).

Further cooling will reduce the distance over which diffusion is effective. Ni left within the *MSS*, particularly within larger grains, may be removed by homogeneous nucleation of orientated lamellae which coarsen into flames. The final stages of exsolution and growth are accompanied by, and assist in, ordering and exsolution within the pyrrhotine grains to give the apparent two phase monoclinic-'hexagonal' intergrowth.

This mechanistic approach, combining experimental work on mechanisms and rates of exsolution with detailed studies of the natural ores, provides the best means of interpreting pyrrhotine/pentlandite intergrowths. With additional work it will be possible to further quantify this model.

Acknowledgements. The Natural Environment Research Council is thanked for provision of a research studentship to D.P.K. Mrs C. Bick is thanked for preparation of the typescript and Ms B. Parker for help with drafting of the diagrams. M. Penstone and U. Purdie of Falconbridge Nickel Mines and A. Bentley of Inco kindly supplied natural samples. W. W. Barker (CSIRO) provided a very useful compilation of published data on the Fe-Ni-S system. J. R. Ashworth (Aston University) gave valuable advice on the manuscript.

REFERENCES

Arnold, R. G. (1967) *Can. Mineral.* **9,** 31–50.

Barrett, F. M., Binns, R. A., Groves D. I., Marston R. J., and McQueen, K. G. (1977). *Econ. Geol.* **72,** 1195–223.

Batt, A. P. (1972) *Can. Mineral.* **11,** 892–7.

Boctor, N. Z. (1981) *Carnegie Inst. Washington Yearb.* **80,** 356–9.

Carpenter, R. H., and Desborough, G. A. (1964) *Am. Mineral.* **49,** 1350–65.

Chadwick, G. A. (1972) *Metallography of Phase Transformations.* Butterworths, London.

Champness, P. E., and Lorimer, G. W. (1976) In *Electron Microscopy in Mineralogy* (H. U. Wenk, ed.), Springer-Verlag.

Condit, R. H., Hobbins, R. R., and Birchenhall, C. E. (1974) *Oxidation of Metals.* **8,** 409–53.

Craig, J. R. (1973) *Am. J. Sci* **273A,** 496–510.

—— and Vaughan, D. J. (1981) *Ore Microscopy and Ore Petrography.* Wiley-Interscience.

Duke, J. M., and Naldrett, A. J. (1978) *Earth Planetary Sci. Lett.* **39,** 255–66.

Durazzo, A., and Taylor, L. A. (1982) *Mineral. Deposita,* **17,** 313–32.

Edwards, A. B. (1947) *Textures of the Ore Minerals.* Aust. Inst. Min. Metall., Melbourne.

Francis, C. A. (1974) A crystallographic study of the $Fe_{1-x}S$-$Ni_{1-x}S$ monosulfide solid solution. M.Sc. thesis, Virginia Polytechnic Inst. and State Univ.

—— Fleet, M. E., Misra, K., and Craig, J. R. (1976) *Am. Mineral.* **61,** 913–20.

Gjostein, N. A. (1973) In *Diffusion.* Am. Soc. Metals, 242–74.

Gresham, J. J., and Loftus-Hills, G. D. (1981) *Econ. Geol.* **76,** 1373–416.
Greenwood, G. W. (1969) In *The Mechanisms of Phase Transformation in Crystalline Solids.* Inst. of Metals (Lond.), 103–10.
Harris, D. C., and Nickel, E. H. (1972) *Can. Mineral.* **11,** 861–78.
Hawley, J. E. (1962) Ibid. **7,** 1–207.
——and Haw, V. A. (1957) *Econ. Geol.* **52,** 132–9.
Kanehira, K. (1969) *Geol. Surv. Can. Paper* 68–5, 79–134.
Klotsman, S. M., Timofeyev, A. H., and Trakhtenberg, I. Sh. (1963) *Phys. Metal. Metallogr.* **16,** 92–8.
Kullerud, G. A. (1963) *Carnegie Inst. Washington Yearb.* **62,** 175–86.
——(1971) In *Research Techniques for High Pressure and High Temperature* (G. C. Ulmer, ed.), Springer-Verlag.
Lear, P. A. (1979) *Spec. Pub. Geol. Soc. S. Africa*, no. 5, 117–32.
McConnell, J. D. C. (1975) *Ann. Rev. Earth Planet. Sci.* **3,** 129–55.
Manning, J. R. (1973) In *Diffusion.* Am Soc. Metals. 1–24.
Marston, R. J., and Kay, B. D. (1980) *Econ Geol.* **75,** 546–65.
Martin, J. W., and Doherty, R. D. (1976) *Stability of Microstructure in Metallic Systems.* Cambridge Univ. Press.
Misra, K. C., and Fleet, M. E. (1973*a*) *Econ. Geol.* **68,** 518–39.
——(1973*b*) *Mater. Res. Bull.* **8,** 669–78.
Morimoto, H., Gyobu, A., Mukaiyama, H., and Izawa, E. (1975) *Econ. Geol.* **70,** 824–33.
Naldrett, A. J. (1979) *Can. Mineral.* **17,** 143–5.
——and Cabri, L. J. (1976) *Econ. Geol.* **71,** 1131–1158.
——Craig, J. R., and Kullerud, G. (1967) Ibid. **62,** 826–47.
Nicholson, R. B. (1970) In *Phase Transformations.* Am. Soc. Metals. 269–309.
Ostwald, J., and Lusk, J. (1978) *Can. J. Earth Sci.* **15,** 501–15.
Papunen, H. (1970) *Ann. Acad. Sci. Fenn.* Ser. AIII, 109.
Polmear, I. J. (1966) *J. Austral. Inst. Metals.* **11,** 246.
Putnis, A., and McConnell, J. D. C. (1980) *Principles of Mineral Behaviour.* Blackwells, Oxford.
Rajamani, V., and Naldrett, A. J. (1978) *Econ. Geol.* **73,** 82–93.
——and Prewitt, C. T. (1973) *Can. Mineral.* **12,** 178–87.
Ramdohr, P. (1969, 1981) *The Ore Minerals and their Intergrowths.* Pergamon, Oxford (1st and 2nd edns.).
Ross, J., and Travis, G. A. (1981) *Econ. Geol.* **76,** 1291–329.
Scott, S. D. (1974) In *Sulfide Mineralogy.* Min. Soc. Am. Short Course Notes, **1,** 51–538.
Shewman, R. W., and Clark, L. A. (1970) *Can. J. Earth Sci.* **7,** 67–85.
Smirnov, V. I. (ed.). (1977) *Ore Deposits of the USSR,* II. Pitman.
Tischler, S. E., Cawthorn, R. G., Kingston, G. A., and Maske, S. A. (1981) *Can. Mineral.* **19,** 607–18.
Uhlmann, D. R., Klein, L., Onorato, P. I. K., and Hopper, R. W. (1975) *Proc. Lunar Sci. Conf. 6th,* 693–705.
Vaughan, D. J., and Craig, J. R. (1978) *Mineral Chemistry of Metal Sulfides,* Cambridge Univ. Press.
——Schwartz, E. J., and Owens, D. R. (1971) *Econ Geol.* **66,** 1131–44.
Wuensch, B. J. (1963) *Mineral. Soc Am. Spec. Pap.* **1,** 157–63.
Yund, R. A., and Hall, H. T. (1970) *J. Petrol.* **11,** 381.
——and McCallister, R. H. (1970) *Chem. Geol.* **6,** 5–30.

[*Revised manuscript received 8 July 1983*]